

This article may be downloaded for personal use only. Any other use requires prior permission of the author and AIP Publishing. This article appeared in *Physics of Fluids*, Vol. 36, Issue 11, 2024 and may be found at <https://doi.org/10.1063/5.0240789>.

Evolution of morphology and electrical properties under controlled flow in polypropylene/polystyrene co-continuous blends containing interfacially localized carbonaceous nanoparticles

Daria Strugova¹, Hind Essadouky¹, Emna Helal^{1,2}, Giovanna Gutierrez², Nima Moghimian², Éric David¹, Nicole R. Demarquette¹ *

¹ Mechanical Engineering Department, École de Technologie Supérieure, Montréal, Québec H3C 1K3, Canada;

² NanoXplore, Inc., 4500 Thimens Boulevard, Saint-Laurent, Quebec H4R 2P2

* Correspondence: NicoleR.Demarquette@etsmtl.ca

Abstract

This study investigates the evolution of morphology and electrical properties of polypropylene (PP)/polystyrene (PS) blend nanocomposites under controlled steady shear flow. These nanocomposites contain either few-layer graphene (FLG) or a mixture of FLG and multi-walled carbon nanotubes (MWCNT), prepared via a conventional melt-mixing. Composites were created by premixing FLG or FLG/MWCNT with either PP (PP/PS/FLG or PP/PS/(FLG+MWCNT)) or PS (PS/PP/FLG or PS/PP/(FLG+MWCNT)) at a PP/PS ratio inducing co-continuous morphology. Results showed a significant reduction in the percolation threshold (PT) for PS/PP/FLG composites, with an 81% decrease compared to PS/FLG. When FLG was premixed with PS, PT required only 2 wt.% FLG, compared to 5.9 wt.% in PP/PS/FLG. Steady shear deformation disrupted the electrical network in both PP/PS/FLG and PS/PP/FLG composites. However, the PS/PP/FLG composites exhibited greater stability in electrical conductivity at lower FLG concentrations (above 3 wt.%) compared to the PP/PS/FLG composites (above 6 wt.%). The applied shear did not affect the co-continuous morphology of the blend-based composites containing 1 wt.% or more of FLG. Additionally, the synergistic effects of the hybrid FLG/MWCNT mixture on the electrical conductivity and rheological properties of both PP/PS/(FLG+MWCNT) and PS/PP/(FLG+MWCNT) composites were evaluated. The incorporation of MWCNT into both PP/PS/FLG and PS/PP/FLG composites significantly enhanced the formation of a hybrid electrical network structure, leading to a further reduction in the percolation threshold concentration of FLG. Specifically, in PP/PS/FLG composites, PT decreased from 5.9 wt.% to 1-3 wt.% of FLG, while in PS/PP/FLG composites, PT dropped from 2 wt.% to 1 wt.% of FLG.

1 Introduction

The incorporation of carbonaceous nanoparticles into dielectric polymers presents substantial potential for a wide range of applications, thanks to their unique properties. While attributes like large specific surface areas, high aspect ratios, and exceptional mechanical strength are inherent to the nanoparticles themselves, they continue to offer significant benefits when embedded in polymer composites. For instance, large surface areas and high aspect ratios can significantly enhance mechanical properties or in the case studied in the present work, electrical conductivity by allowing the formation of electrically conductive networks more easily. Therefore, the benefits of these nanoparticles' properties are indeed transferred to the composites. It has been extensively demonstrated that introducing carbon nanotubes (CNT) [1-12], carbon black (CB) [13-23], or graphene [24-33] into polymer blends with co-continuous morphologies can enhance the electrical properties of these composites. The introduction of electrically conductive fillers into co-

This is the author's peer reviewed, accepted manuscript. However, the online version of record will be different from this version once it has been copyedited and typeset.

PLEASE CITE THIS ARTICLE AS DOI: 10.1063/1.50240789

continuous polymer blends is particularly effective in lowering the percolation threshold concentration through the double percolation effect [1-3, 7, 34-38]. The percolation threshold represents the critical concentration of nanoparticles at which the material transitions from an insulator to a conductor. This threshold is achieved when the filler is strategically located within one of the polymer phases or at the interface between the two polymers that form the co-continuous morphology.

To obtain conductive nanocomposites, carbon nanotubes (CNT) have attracted significant attention due to their outstanding electrical conductivity [1, 4, 12, 39]. However, the production of CNT typically involves chemical vapor deposition, which can be relatively expensive. In contrast, graphene, which is derived from graphite, offers a possible more cost-effective alternative. Graphene nanoplatelets (GNP) have also garnered substantial interest due to their two-dimensional structure and large specific surface area, making them a promising candidate as an electrically conductive additive.

Recently, there has been an increasing focus on developing hybrid polymer nanocomposites that combine different types of carbon nanoparticles to achieve synergistic effects and reduce costs. The literature indicates that combining carbon nanomaterials with distinct geometries can enhance the conductive network within these hybrid nanocomposites. For example, studies have investigated the synergistic effects on the electrical properties of composites containing GNP and CNT [40-49] or carbon black (CB) and CNT [47, 50]. One notable example is the work by Xiao et al. [40], who demonstrated that the addition of 2 wt.% CNTs to polyvinylidene difluoride (PVDF)/GNP composites produced a synergistic effect, leading to a significant reduction in the percolation threshold concentration for GNP from 20 wt.% to 5 wt.%. This reduction is attributed to the formation of a 3D hybrid network structure within the PVDF/CNT/GNP composites. Similarly, Kuester et al. [41] found that in hybrid nanocomposites of styrene ethylene butylene styrene block copolymer (SEBS)/GNP/CNT with CNT loadings of 8 wt.% or higher, the electrical conductivity leveled off, with a synergistic effect observed in composites containing GNP and CNT in weight ratios of 7/3 wt.% and 5/5 wt.%.

To date, only a limited number of studies have explored the synergistic effects of mixing carbonaceous particles on the electrical conductivity of polymer blend-based composites [35, 36, 51, 52]. For instance, Dos Anjos et al. examined the impact of adding CNT on the electrical and electromagnetic shielding properties of hybrid nanocomposites composed of a polycarbonate (PC)/acrylonitrile butadiene styrene (ABS) blend with GNP and CNT. They found that the addition of 1.5 wt.% CNT to the PC/ABS/GNP blend significantly reduced the percolation threshold concentration for GNP from 10 wt.% to 3 wt.%, while simultaneously enhancing electrical conductivity [51].

However, during the processing of these composites, the materials are subjected to deformation, which can alter their morphology. The preservation of co-continuous morphology is critical, as it enables the achievement of the desired electrical conductivity at the lowest possible filler concentration. Therefore, maintaining stable morphology during further processing steps is essential to preserving the electrical properties of the composites. This becomes particularly important in the context of recycling, where repeated processing can degrade the material structure. Ensuring stability during recycling not only supports material reuse but also minimizes the need for additional filler to restore electrical performance.

Our previous work demonstrated that it is possible to achieve a very low percolation threshold in a polypropylene/polystyrene/MWCNT system by employing various thermal treatments, reaching a threshold as low as ~0.06 wt.% MWCNT [53]. However, we also found that only a substantial

This is the author's peer reviewed, accepted manuscript. However, the online version of record will be different from this version once it has been copyedited and typeset.

PLEASE CITE THIS ARTICLE AS DOI: 10.1063/1.5240789

concentration of MWCNT (~1 wt.%) could stabilize the co-continuous morphology and, consequently, the electrical conductivity of such composites when subjected to deformation [54]. This deformation leads to changes in both the blend morphology (resulting in coarsening) and the electrical network, which increases both rheological and electrical percolation thresholds.

To investigate the effect of deformation on the electrical and morphological properties of these composites, small amplitude oscillatory shear (SAOS) tests, followed by the deformation and subsequent SAOS tests, can be performed [54-62]. SAOS tests conducted in the linear viscoelastic region allow for the characterization of the equilibrium morphology of binary blends before and after the steady shear deformation, using established constitutive models [2, 16, 62-69]. These tests enable the monitoring of morphological evolution during the deformation.

In a previous study, we investigated nanocomposites of PP/PS/MWCNT, where MWCNT was initially mixed with PP to promote selective MWCNT diffusion from PP to PS, assessing the impact of steady shear deformation on the morphological and electrical properties of this model system [54]. In the current work, we prepared PP/PS/FLG composites by premixing FLG with PP to facilitate selective FLG diffusion from PP to PS nanocomposites. Additionally, we prepared PS/PP/FLG composites by premixing FLG with PS to lock the co-continuous morphology, as FLG is thermodynamically unfavorable to diffuse into PP. Furthermore, we investigated hybrid nanocomposites of PP/PS/(FLG+MWCNT) and PS/PP/(FLG+MWCNT) to assess the synergistic effects of FLG and MWCNT on the electrical conductivity of co-continuous blend-based composites. All composites were fabricated using the same conventional melt-mixing process.

In this study, PP/PS/FLG and PS/PP/FLG composites exhibiting double percolation, with FLG concentrations of up to 9 wt.%, as well as PP/PS/(FLG+MWCNT) and PS/PP/(FLG+MWCNT) hybrid composites were subjected to a series of SAOS-steady shear-SAOS tests to examine the evolution of co-continuous morphology and electrical properties under controlled flow conditions. The steady shear rate applied during deformation was selected to promote the break-up of the morphology. The blend morphology evolution during deformation was evaluated using rheological model and scanning electron microscopy. The electrical properties of the materials were monitored throughout the deformation process and were linked to the morphological changes. Additionally, the potential for recovery of morphological and electrical properties after deformation was explored.

2 Materials and Methods

2.1 Materials

In this study, PP (PP4712E1 grade) was purchased from ExxonMobil, and PS (MC3650 grade) was purchased from PolyOne. Their respective characteristics are detailed in Table 1. Few-layer graphene (FLG) powder (GrapheneBlack 3X grade) was provided by NanoXplore Inc. This grade of FLG typically consists of 6 to 10 atomic layers. The primary particles exhibit a lateral size ranging from 1 to 2 μm . Additionally, MWCNT (NC7000™ grade), with an average diameter of 9.5 nm, a length of 1.5 μm , and a nominal electrical conductivity of $10^6 \text{ S}\cdot\text{m}^{-1}$, was purchased from Nanocyl.

This is the author's peer reviewed, accepted manuscript. However, the online version of record will be different from this version once it has been copyedited and typeset.

PLEASE CITE THIS ARTICLE AS DOI: 10.1063/1.5240789

Table 1. Properties of polymers.

Polymers	M_w (g/mol)	M_w/M_n	Density ($\text{g}\cdot\text{cm}^{-3}$)	η_0 (Pa·s) at 200 °C
PP	317 420	6.65	0.9	7 800
PS	105 000	2.37	1.04	4 080

* η_0 – zero-shear viscosity. Zero-shear viscosity of neat PP and PS was found by fitting the experimental data to the Carreau model [70, 71].

2.2 Composites preparation

The materials were prepared using a melt-mixing process with a Haake Rheomix OS PTW16 twin-screw extruder (Thermo Fisher Scientific Inc., Waltham, MA, USA). The temperature was set to 220°C across all 10 zones and the die, with a screw speed of 100 rpm for all compositions.

First, masterbatches of PP/FLG and PS/FLG with 21 wt.% FLG, and PP/MWCNT and PS/MWCNT with 10 wt.% MWCNT, were prepared. The PP/FLG and PS/FLG masterbatches were diluted with pure PP and pure PS, respectively, to produce composites containing 2, 6, 10, and 16 wt.% FLG. Then, the PP/FLG composites were further diluted with both PP and PS to obtain PP/PS/FLG composites with 1, 3, 6, and 9 wt.% FLG (with FLG first premixed with PP), achieving a co-continuous morphology with 50/50 wt.% of the PP/PS blend. The same procedure was followed to produce PS/PP/FLG composites (with FLG first premixed with PS).

The same process was used to create hybrid PP/PS/(FLG+MWCNT) and PS/PP/(FLG+MWCNT) composites. A summary of all prepared composites is listed in Table 2.

To achieve a co-continuous morphology in PP/PS blend-based filled composites, the co-continuous range must be calculated based on viscosity measurements of both PP and PS. The viscosity of PP and PS was measured using a capillary rheometer (SR20, Instron) at 220 °C across a range of high shear rates (10 to 1000 s^{-1}). The measurements were conducted using a capillary with a length of 40 mm and a diameter of 1 mm. At an effective shear rate of 100 s^{-1} , which is experienced in the twin-screw extruder, both polymers exhibited similar viscosities [72, 73]. Additionally, the volume fraction of each phase was calculated using the melt density of both PP and PS. A 50/50 wt.% PP/PS concentration was chosen based on the analysis by Jordhamo, G. et al. [74].

Table 2. FLG and MWCNT weight % in PP/PS/filler composites.

Composites	FLG, wt.%	MWCNT, wt.%
PP/FLG	0 – 16	–
PS/FLG	0 – 16	–
PP/PS/FLG	0 – 9	–
PS/PP/FLG	0 – 9	–
PP/PS/(FLG+MWCNT)	1 – 3	0.1 – 0.3
PS/PP/(FLG+MWCNT)	1	0.1 – 0.3

2.3 Characterization

2.3.1 Rheological analysis

The rheological properties of the composites were assessed using an Anton Paar MCR 501 rotational rheometer in a dry nitrogen atmosphere. Measurements were performed with parallel-plates geometry (1 mm gap, 25 mm diameter) at 200 °C. To determine the linear viscoelastic

(LVE) region, dynamic strain sweep tests (DSST) were conducted for all composites at three different angular frequencies, 1, 10, and 100 rad/s, in a strain range from 0.01 to 10 %. A strain of 0.3% was selected for subsequent tests, aligning with the LVE region. Small amplitude oscillatory shear (SAOS) tests were then conducted to investigate morphology evolution. Morphology evolution was studied by performing sequences of SAOS tests, followed by steady shear, and another SAOS, as depicted in Figure 1(a) of our previous work [54]. Steady shear tests were performed at a rate of 1 s^{-1} for a shear deformation of 250%. This shear rate was chosen to be high enough to induce morphology and filler network deformation but low enough to prevent edge failure and sample ejection from the plate-plate geometry [69].

Despite the non-uniform shear rate in parallel-plates geometry, it was chosen for simultaneous measurement of electrical properties and rheological properties under deformation. This geometry also allowed bulk property analysis, which is crucial for understanding morphological evolution. For a comprehensive view of the co-continuous morphology, samples for scanning electron microscopy were taken after applied steady shear deformation and broken along the diameter and examined at a fixed position from the center. More details can be found in Methodology Section of our previous work [54].

2.3.2 Electrical conductivity analysis

Dielectro-rheological device (DRD)

Electrical characterization of all composites at the molten state was performed during both steady shear and time sweep (annealing) steps using the MCR501 rheometer equipped with a dielectro-rheological device (DRD with ST2826/A high-frequency LCR meter). This setup allows for simultaneous rheological and electrical measurements. The parameters for the steady shear tests are detailed in the Rheological Analysis section. The time sweep, needed for stress relaxation step, was conducted at an angular frequency of 0.05 rad/s. Electrical properties were measured by applying a 20 Hz AC signal with 1 V_{RMS} across the sample. The deformation history performed for electrical conductivity measurements is presented in Figure 1.

The electrical conductivity at 200 °C was evaluated from the real part of the complex conductivity given by:

$$\sigma' = \frac{1}{R_p} \frac{d}{A} \quad (1)$$

where R_p is the equivalent parallel resistance, A is the plate area, and d is the distance between the plates. This parameter can then be expressed as a function of the direct conductivity by:

$$\sigma'(\omega) = \sigma + \omega \varepsilon_0 \varepsilon'' \quad (2)$$

where σ is the direct current conductivity, referred simply as the electrical conductivity, ε'' is the dielectric losses related to relaxation mechanisms and ω is the electrical angular frequency (40π rad/s in the case of the dielectro-rheological device). In practical, as soon as the material starts to be even slightly conductive, the first term of equation (2) - σ becomes dominant and σ' can be considered equivalent to the true conductivity.

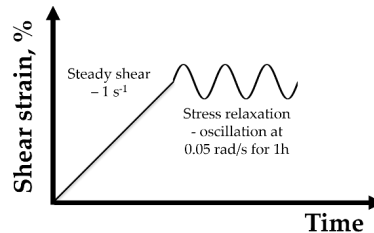


Figure 1 – deformation history for electrical conductivity measurements by using DRD cell coupled with rheometer.

Broadband dielectric spectrometer (BDS)

At room temperature, the electrical conductivity of the composites was measured using a broadband dielectric spectrometer (BDS) from Novocontrol Technologies GmbH & Co. KG, Montabaur, Germany. Measurements were taken over a frequency range of 10^{-2} to 3×10^5 Hz with an excitation voltage of 1 V_{RMS} applied across the sample. The method for calculating electrical conductivity from the complex capacitance is detailed in our previous work [53]. In the same way as mentioned previously for the dielectro-rheological device, the electrical conductivity was evaluated from the real part of the complex conductivity $\sigma'(\omega)$, but at a lower frequency of 10^{-2} Hz. For these measurements, disks 25 mm in diameter and 1 mm thick, coated with 20 nm of gold on both sides using a gold sputter coater (model K550X) to ensure better contact with the electrodes, were used.

2.3.3 Microscopy analysis

The morphology of polymer blend-based composites was observed using scanning electron microscopy (SEM) with a Hitachi S3600 microscope (Hitachi, Ltd., Tokyo, Japan) in secondary electron mode. The samples were fractured in liquid nitrogen, and the polystyrene phase was extracted using 2-butanone solvent at room temperature under continuous stirring for four hours. After extraction, the samples were dried under vacuum at room temperature for 12 hours. Subsequently, the samples were coated with gold using a gold sputter coater (model K550X). All porous samples, following PS extraction, were imaged at an accelerating voltage of 5 kV.

3 Results

3.1 Electrical conductivity

3.1.1. Electrical properties of PP/PS/FLG and PS/PP/FLG composites

Figure 2 shows the electrical conductivity as a function of FLG weight fraction for PP/FLG and PS/FLG composites, as well as PP/PS/FLG and PS/PP/FLG blend-based composites, where FLG was first premixed with PP and PS, respectively. Here, the percolation threshold concentrations for all composites were evaluated using Equation (3) and the data presented in Figure 2.

$$\sigma = k \cdot (p - p_c)^t, \text{ with } p > p_c, \quad (3)$$

where σ is the electrical conductivity of chosen composite with different filler concentration, p is the mass fraction of FLG, p_c is the percolation threshold concentration, t is a fitted exponent that

depends, only, on the dimensionality of the system, and k is a scaling factor. The fitting parameters are presented in Table 3.

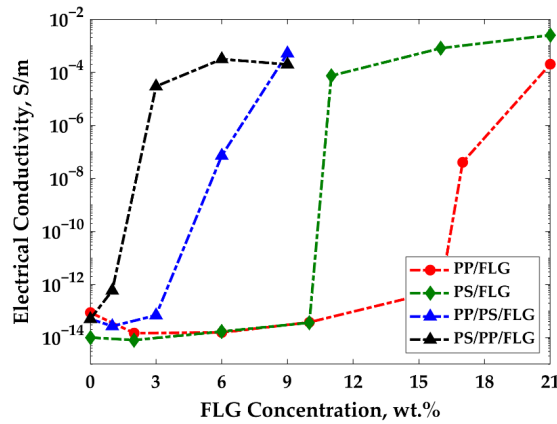


Figure 2 – Electrical conductivity as a function of filler weight fraction for PP/FLG, PS/FLG, PP/PS/FLG and PS/PP/FLG composites.

Table 3. Percolation threshold and fitting values of experimental data according to Equation (3) for each composite studied in this work.

Parameters	PP/FLG	PS/FLG	PP/PS/FLG	PS/PP/FLG
p_c , wt.%	16.8	10.4	5.9	2
k , S/m	4.3×10^{-6}	1.2×10^{-4}	3.2×10^{-5}	3.3×10^{-5}
t	2.7	1.1	2.7	1
R^2	0.99	0.98	0.99	0.99

In this work, two approaches were used to achieve a reduction in the percolation threshold concentration. The first approach involved adding FLG or FLG+MWCNT in the less favorable phase to induce filler diffusion toward the polymer blend interface, potentially resulting in the lowest possible percolation threshold concentration. The second approach involved adding FLG or FLG+MWCNT in the more favorable phase to reduce the percolation threshold concentration compared to single matrix composites and to stabilize the polymer blend morphology. This approach is based on the idea that the filler will remain in one phase and not diffuse due to thermodynamically driven diffusion, which should prevent the continuous phase from coarsening. The prediction of FLG and MWCNT affinity to one of the phases or the interphase was made using Young's equation to estimate the wetting coefficient (ω_a) [7, 75, 76].

The results, presented in Table 3, show that the percolation threshold for the PP/PS/FLG composite was reduced by 65% compared to PP/FLG composites (from 16.8 wt.% to 5.9 wt.% FLG), and for the PS/PP/FLG composite, it was reduced by 81% compared to PS/FLG composites (from 10.4 wt.% to 2 wt.% FLG). The reduction in percolation threshold was more significant when FLG was first mixed with the more favorable PS phase.

There are two main reasons for this effect. First, it is challenging to tailor the location of the filler at the interface between two polymers using a conventional melt-mixing process. Second, the crystallization effect in semi-crystalline polymers, where the filler is placed in case of PP/PS/FLG composites, can influence electrical conductivity. During cooling, small crystals of PP grow on the filler particles, which are acting as nuclei [77-79]. This creates an insulating layer surrounding the particles and preventing them from forming an electrically conductive network. This does not occur when the filler is located in an amorphous PS phase in case of PS/PP/FLG composites.

However, it is possible further reduce PT concentration in PP/PS/FLG composites. There is another mechanism that may contribute to increased electrical conductivity which involves the influence of growing PP crystals on the creating electrically conductive nanoparticles network. As PP crystals grow, they may exert pressure on the conductive fillers, pushing them through the amorphous regions of the polymer matrix. This movement could result in a denser, more interconnected conductive network, potentially lowering the percolation threshold.

We have previously investigated this effect in an earlier study [53], where the volume exclusion effect of PP crystals on MWCNT was examined. By promoting the growth of large PP crystals using both isothermal (holding the sample at a chosen constant temperature) and non-isothermal (slow cooling from the molten state) thermal annealing, we observed that the growing PP crystals pushed the MWCNT towards their boundaries, which helped to create a denser, more robust electrically conductive network. While we did not aim to apply any specific thermal treatments in the current work, such an approach could potentially achieve a similar effect by enhancing the formation of a conductive FLG or FLG+MWCNT network.

3.1.2 Synergistic effect of FLG and MWCNT on electrical conductivity of PP/PS/(FLG+MWCNT) and PS/PP/(FLG+MWCNT) co-continuous blends

Figure 3 (a) presents the electrical conductivity as a function of filler weight concentration for all hybrid composites of PP/PS/(FLG+MWCNT) and PS/PP/(FLG+MWCNT), where FLG and MWCNT were first premixed with PP and PS, respectively. These are compared with the PP/PS/FLG and PS/PP/FLG blend-based composites. Figure 3 (b) shows the real part of the complex electrical conductivity as a function of frequency for chosen PP/PS/(FLG+MWCNT) hybrid composites. The FLG and MWCNT concentrations for the hybrid systems were selected based on the electrical conductivity data in Figure 2 for both PP/PS/FLG and PS/PP/FLG, and on the data presented in Figure 2 of our previous work for PP/PS/MWCNT composites (fast cooling treatment) [53]. It can be observed that PP/PS/FLG is not conductive at 1 wt.% and 3 wt.% FLG. Therefore, these two concentrations were chosen to investigate the synergistic effect of FLG and MWCNT on electrical conductivity of PP/PS/FLG composites. Specifically, 0.1 wt.% and 0.3 wt.% MWCNT were added to PP/PS/FLG containing 1 wt.% and 3 wt.% FLG, respectively. The same approach was applied to the PS/PP/FLG composite, where 0.1 wt.% and 0.3 wt.% MWCNT were added to PS/PP/FLG containing 1 wt.% FLG, as it was not conductive at this FLG concentration. The MWCNT concentrations of 0.1 wt.% and 0.3 wt.% were chosen based on the observation that PP/PS/MWCNT with 0.1 wt.% MWCNT is not conductive, while 0.3 wt.% MWCNT is the percolation threshold concentration for the PP/PS/MWCNT composite.

The results indicate that the addition of both FLG and MWCNT resulted in a synergistic effect on electrical conductivity for the co-continuous polymer blends studied in this work. This was true whether the fillers were incorporated in PP or PS phase. Specifically, the electrical conductivity increased by 8 and 9 orders of magnitude when 1 wt.% FLG was combined with 0.1 wt.% and 0.3 wt.% of MWCNT, respectively (see the results presented in Table 4). This significant enhancement

This is the author's peer reviewed, accepted manuscript. However, the online version of record will be different from this version once it has been copyedited and typeset.

PLEASE CITE THIS ARTICLE AS DOI: 10.1063/1.5240789

is compared to the electrical conductivity of PP/PS/FLG containing only 1 wt.% of FLG and PP/PS/MWCNT containing only 0.1 wt.% and 0.3 wt.% of MWCNT. The same effect was observed in PS/PP/(FLG+MWCNT) containing 1 wt.% of FLG and 0.1 wt.% of MWCNT. In this case electrical conductivity increased by 6 orders of magnitude (see the results presented in Table 5).

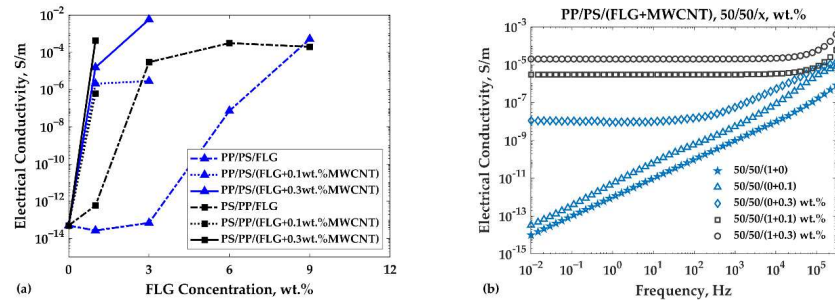


Figure 3 – (a) Electrical conductivity as a function of filler weight concentration for PP/PS/FLG and PS/PP/FLG composites, and PP/PS/(FLG+MWCNT) and PS/PP/FLG(FLG+MWCNT) hybrid composites and (b) Real part of the complex conductivity as a function of frequency for chosen PP/PS/(FLG+MWCNT) composites.

The drastic increase in conductivity can be attributed to the formation of an efficient conductive network facilitated by the combined presence of FLG and MWCNT. FLG, with its large surface area and high aspect ratio, provides an extensive conductive pathway. Meanwhile, MWCNT, known for its high electrical conductivity, bridges the gaps between FLG particles, creating a more interconnected network [40-43, 48-51]. This combination effectively lowers the percolation threshold and enhances the overall conductivity of the composite.

Table 4. FLG + MWCNT synergetic effect on electrical conductivity of PP/PS/FLG co-continuous blend.

FLG, wt. %	PP/PS/FLG, σ , S/m	MWCNT, wt. %	PP/PS/MWCNT, σ , S/m	PS/PP/(FLG+MWCNT), σ , S/m
1	3×10^{-14}	0.1	3.4×10^{-14}	3×10^{-6}
1	3×10^{-14}	0.3	1.1×10^{-8}	2×10^{-5}
3	7×10^{-14}	0.1	3.4×10^{-14}	2.9×10^{-6}
3	7×10^{-14}	0.3	1.1×10^{-8}	6×10^{-3}

Table 5. FLG + MWCNT synergetic effect on electrical conductivity of PS/PP/FLG co-continuous blend.

FLG, wt. %	PS/PP/FLG, σ , S/m	MWCNT, wt. %	PS/PP/MWCNT, σ , S/m	PS/PP/(FLG+MWCNT), σ , S/m
1	6×10^{-13}	0.1	6.9×10^{-13}	6.2×10^{-7}
1	6×10^{-13}	0.3	1.5×10^{-5}	4×10^{-4}

3.2 Effect of adding FLG and MWCNT on morphology and rheological properties of co-continuous blends

In terms of rheological properties, it is important to track the storage modulus of filled composites, as its behavior at low frequencies plays a key role in determining the system's overall elasticity. Studies have consistently shown that, regardless of the composite matrix's complexity, the rigid filler network's impact on the elastic modulus becomes more significant at lower frequencies compared to the matrix alone [80-82]. Figures 4(a-b) present storage modulus as a function of frequency for both PP/PS/FLG composites with varying FLG concentrations and selected PP/PS/(FLG+MWCNT) hybrid composites. The data reveal that the storage modulus of the blend at low frequencies is higher than that of the individual pure components. This increase in storage modulus in polymer blends is attributed to the additional stress contribution from the deformation of the interface [64]. Additionally, the results show that the storage modulus increases with FLG concentration above 3 wt.% at low frequencies, displaying a plateau that signifies solid-like behavior due to the formation of a rigid nanoparticle network [2, 4, 26]. For hybrid composites, the storage modulus of the PP/PS/(FLG+MWCNT) composite, containing only 1 wt.% of FLG and 0.3 wt.% of MWCNT, already exhibits a plateau, which indicates a formation a rigid filler network at lower concentration of FLG. Furthermore, in the case of PP/PS/(FLG+MWCNT) composite with 1 wt.% FLG and 0.1 wt.% MWCNT, the storage modulus is higher than that of the PP/PS/FLG composite with 1 wt.% FLG and the PP/PS/MWCNT composites with 0.1-0.3 wt.% MWCNT. This observation underscores the synergistic effect of the combined filler network on the rheological properties of the system.

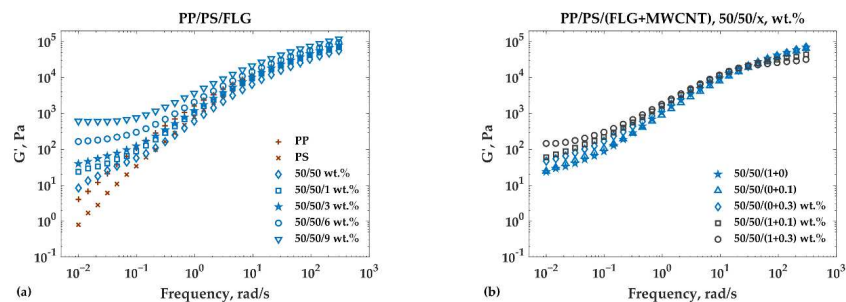


Figure 4 – Storage moduli as a function of frequency for: (a) PP/PS/FLG composites and (b) for chosen PP/PS/(FLG+MWCNT) composites.

Figures 5(a-e) illustrate the co-continuous morphology of selected PP/PS/FLG and PS/PP/FLG composites with the addition of 0 wt.%, 3 wt.%, and 9 wt.% FLG. The results suggest that adding FLG significantly refines the co-continuous morphology, especially when FLG is premixed with PS. In PP/PS/FLG composites, higher concentrations of FLG were required to achieve a similar refinement. Figure 6(a-f) demonstrates the synergistic effect of FLG and MWCNT on the co-continuous morphology of selected PP/PS/(FLG+MWCNT) composites. It is evident that adding 0.3 wt.% MWCNT to a PP/PS/FLG composite containing 1 wt.% FLG suppresses the coarsening of the co-continuous morphology, transforming it from a mixed droplet-like and rod-like structure to a fine co-continuous one. Furthermore, for a PP/PS/FLG composite with 3 wt.% FLG, the addition of just 0.1 wt.% MWCNT was sufficient to refine the co-continuous morphology.

This is the author's peer reviewed, accepted manuscript. However, the online version of record will be different from this version once it has been copyedited and typeset.

PLEASE CITE THIS ARTICLE AS DOI: 10.1063/1.50240789

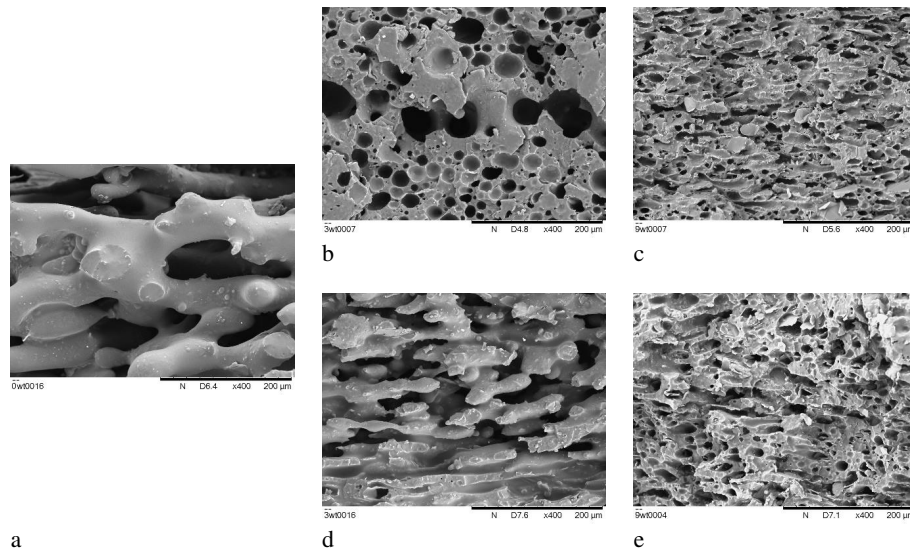
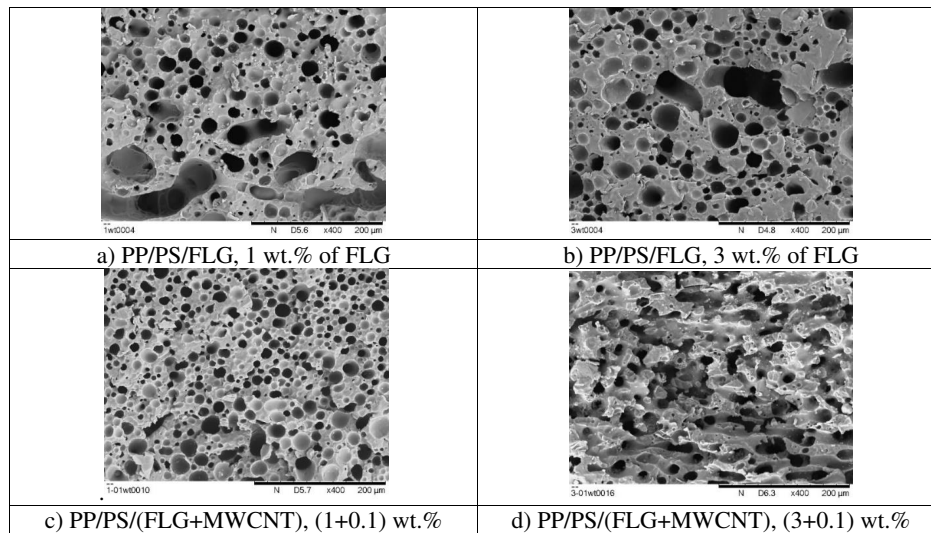


Figure 5 – Morphology evolution of selected PP/PS/FLG and PS/PP/FLG composites for: (a) 0 wt.% of FLG; (b-c) PP/PS/FLG with 3 wt.% and 9 wt.% of FLG, respectively; and (d-e) PS/PP/FLG with 3 wt.% and 9 wt.% of FLG, respectively.



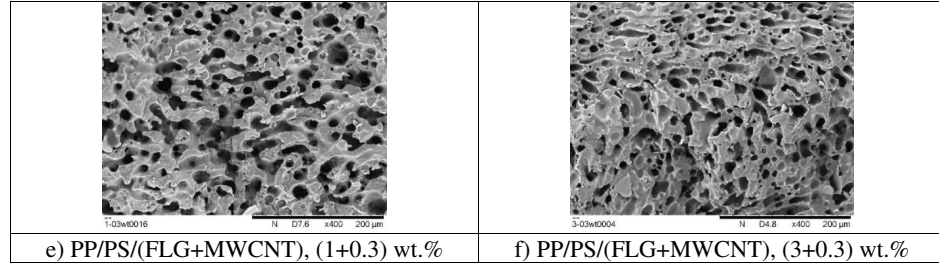


Figure 6 – Morphology evolution of selected PP/PS/(FLG+MWCNT) composites, containing different weight concentration of FLG and MWCNT.

In order to quantify the co-continuous morphology of the polymer composites, the characteristic domain size can be calculated using two primary methods: image analysis via scanning electron microscopy (SEM) and model fitting to rheological data. The first method involves capturing high-resolution SEM images of the composite's morphology and analyzing these images to determine the characteristic domain size. The calculation is performed using Equation (4) [25, 26]:

$$\xi = \frac{A_{SEM}}{L_{int}} \quad (4)$$

where A_{SEM} represents the total area of the SEM image (see Figure 5, for example), and L_{int} denotes the interface length between the PP and PS phases. The interface length is estimated using a custom image analysis script written in MATLAB. This script processes the SEM images and calculates the perimeter of the interface, providing a measure of the interfacial length. The analyses were carried out on at least 10 images to ensure statistical reliability. The MATLAB code for this image treatment and interface length calculation was developed based on the methodology described by Galloway et al. [83].

The second method for quantifying the co-continuous morphology involves using rheological measurements to infer the domain size by fitting experimental data to theoretical model. This approach utilizes small amplitude oscillatory shear (SAOS) tests to characterize the rheological behavior of the filled blend-based composites with a co-continuous morphology. The data is then fitted to a modified Yu et al. (YZZ) model, as described in Equation (4) [62]:

$$G'_{blend}(\omega) = G'_{components}(\omega) + G'_{interface}(\omega) + G'_0 \quad (5)$$

In this equation: $G'_{components}(\omega)$ represents the contribution of the individual components within the blend. This term can be calculated using Equation (4) from reference [84], which considers the storage moduli of each polymer in the blend and the geometrical parameters of a simplified co-continuous morphology. $G'_{interface}(\omega)$ denotes the contribution of the interface between the polymer phases. This term is computed using Equation (15) from reference [68], which incorporates both the geometrical parameters of the co-continuous morphology and the physical properties of the blend components, such as the viscosity of each polymer and the interfacial tension between them. G'_0 is an adjustable constant that accounts for the rigidity of the filler network within the composite. This parameter is included to capture the additional stiffness

This is the author's peer reviewed, accepted manuscript. However, the online version of record will be different from this version once it has been copyedited and typeset.

PLEASE CITE THIS ARTICLE AS DOI: 10.1063/1.50240789

imparted by the fillers and is described in references [62, 69]. More detailed description of the model can be found in the works of Yu et al. and Strugova et al. [62, 68]. The characteristic domain size of selected PS/PP/FLG composites was calculated using the two methods described earlier. Figure 7 (a-b) illustrates the characteristic domain size of the selected PS/PP/FLG and PP/PS/(FLG+MWCNT) composites. The data reveal that the addition of FLG significantly reduces the characteristic domain size, decreasing from 12.7 μm in the neat PP/PS blend to 1.6 μm in the PS/PP/FLG composite with 9 wt.% FLG. Notably, the characteristic domain size does not exhibit substantial variation for PS/PP/FLG composites with FLG concentrations ranging from 3 wt.% to 9 wt.%, remaining between 3 μm and 1.6 μm . However, it is evident that the addition of only 1 wt.% FLG is insufficient to refine the co-continuous morphology, as the characteristic domain size remains comparable to that of the neat PP/PS blend. In the case of hybrid composites, the incorporation of FLG and MWCNT into either the PP or PS phases helps stabilize the polymer blend morphology. When FLG and MWCNT are dispersed within the same phase, they interact synergistically, promoting a uniform distribution and preventing phase separation. It can be seen that the addition of 0.1 wt.% MWCNT to a PP/PS/FLG composite containing 3 wt.% FLG significantly reduces the domain size from 7.5 μm to 2 μm , indicating a refinement of the co-continuous morphology. Further increases in MWCNT concentration do not significantly affect the domain size.

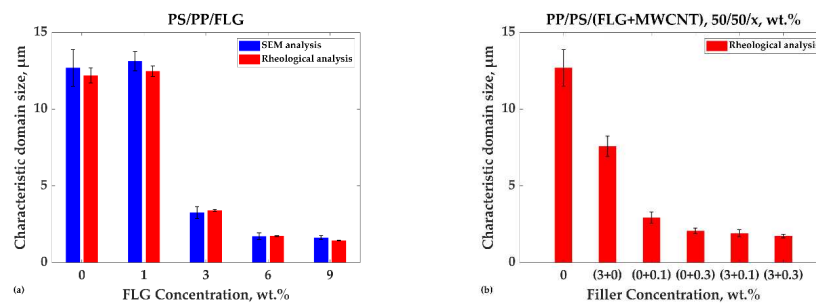


Figure 7 - Characteristic domain size as a function of FLG concentration, calculated by using both SEM and rheological analysis for (a) PS/PP/FLG composites and (b) for chosen PP/PS/(FLG+MWCNT) composites (calculated by using rheological analysis).

3.3 Effect of steady deformation on electrical conductivity and morphology

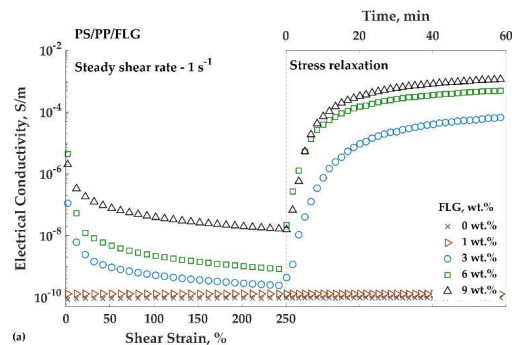
Figure 8(a-c) illustrates electrical conductivity as a function of shear strain for composites subjected to deformation at a steady shear rate of 1 s^{-1} , and as a function of time during the subsequent stress relaxation step for (a) PS/PP/FLG and (b) PP/PS/FLG composites, and (c) PP/PS/(FLG+MWCNT) hybrid composites. The data reveals that for PS/PP/FLG composites with FLG concentrations equal to or above 3 wt.%, there is a significant increase in electrical conductivity during the stress relaxation phase (see results presented in Table 6). This recovery follows a substantial reduction in conductivity, by several orders of magnitude, induced by the applied steady shear deformation. Remarkably, the electrical conductivity returns to the values observed prior to the shear deformation and stress relaxation step for both composites (as detailed in Table 6).

In contrast, for the PP/PS/FLG composites, the stabilization of electrical conductivity after steady shear deformation is observed at a higher FLG concentration of 6 wt.%. This threshold aligns with

This is the author's peer reviewed, accepted manuscript. However, the online version of record will be different from this version once it has been copyedited and typeset.

PLEASE CITE THIS ARTICLE AS DOI: 10.1063/1.50240789

the percolation threshold concentration for this set of composites, at which the composites exhibit stable, high electrical conductivity and a well-maintained fine co-continuous morphology. The reduction in electrical conductivity during the applied steady shear deformation can be attributed to the disruption of the FLG conductive network and the coarsening of the matrix blend morphology. As the matrix coarsens, the previously co-continuous morphology can transform into a drop-in-matrix type morphology, which is less favorable for electrical conductivity. The continuity of morphology is a crucial factor for maintaining high electrical conductivity and achieving a low percolation threshold. These changes are influenced by three key factors: FLG concentration, the strain applied, and the shear rate. A higher concentration of FLG helps maintain a more robust network, while the applied strain and shear rate can impact the degree of disruption and reformation of the conductive network within the composite. However, in the case of PP/PS(FLG+MWCNT) composites, the addition of just 0.3 wt.% MWCNT combined with 1 wt.% FLG is sufficient to fully restore electrical conductivity. And for a PP/PS/FLG composite containing 3 wt.% FLG, adding only 0.1 wt.% MWCNT is enough to fully recover electrical conductivity after deformation (as detailed in Table 7). As previously concluded, it is possible to reduce the percolation threshold concentration in PP/PS/FLG composites from 6 wt.% to 1-3 wt.% FLG by incorporating only 0.1 wt.% MWCNT. Interestingly, after the applied shear deformation, PP/PS(FLG+MWCNT) hybrid composites demonstrate faster recovery of electrical conductivity and at lower FLG concentrations compared to PP/PS/FLG or PS/PP/FLG composites. This suggests that the hybrid networks formed in these systems are more robust. The quicker recovery can be attributed to specific interactions between FLG and MWCNT, and their ability to re-orient during the stress relaxation step, even though this step occurs at a low oscillation frequency of 0.05 rad/s. These findings indicate a strong relationship between the percolation threshold and the stabilization of electrical conductivity in these composites. The re-establishment of conductivity during the stress relaxation phase suggests that the FLG network within the composite reconstructs itself after being disrupted by shear deformation. The differences in the stabilization concentrations between PS/PP/FLG and PP/PS/FLG composites likely arise from distinct filler distributions and interactions within the polymer phases, which affect the robustness and efficiency of the conductive networks formed.



This is the author's peer reviewed, accepted manuscript. However, the online version of record will be different from this version once it has been copyedited and typeset.

PLEASE CITE THIS ARTICLE AS DOI: 10.1063/1.50240789

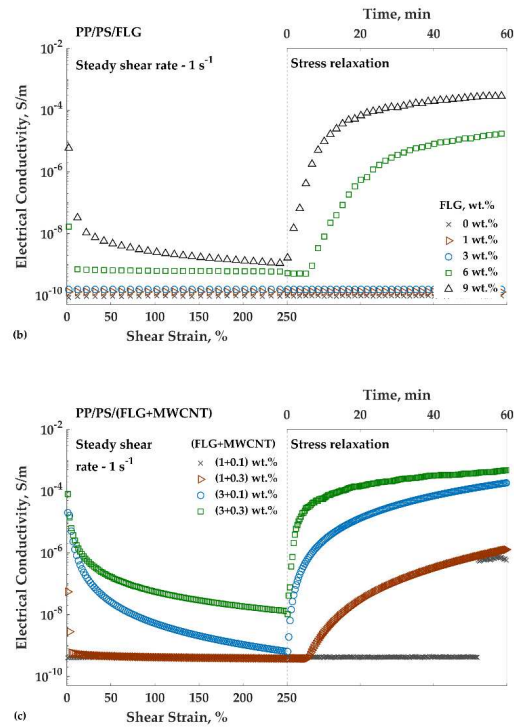


Figure 8 – Electrical conductivity vs shear strain at a steady shear step and as a function of time at a stress relaxation step for (a) PS/PP/FLG and (b) PP/PS/FLG composites, and (c) PP/PS/(FLG+MWCNT) hybrid composites.

Table 6 and Table 7 present the electrical conductivity data for PS/PP/FLG and PP/PS/FLG composites, and PP/PS/(FLG+MWCNT) hybrid composites, respectively, under three conditions: (1) prior to any deformation, with measurements obtained from BDS at 25 °C, (2) after the application of 250% steady shear deformation at a shear rate of 1 s⁻¹, and (3) following a 1-hour recovery period at 200 °C, with the latter two measurements obtained using the DRD cell coupled with the rheometer.

It is important to note that the LCR meter coupled with the rheometer in this study has limited sensitivity for highly dielectric materials unlike the dielectric spectrometer. Specifically, it is unable to measure electrical conductivity below 1×10^{-10} S/m. Consequently, all composites containing 0 wt.% and 1 wt.% of FLG display the same conductivity values, as the device cannot detect differences at these low conductivity levels. However, for higher conductivity measurements, the device provides sufficiently accurate results.

Table 6. Electrical conductivity data for PS/PP/FLG and PP/PS/FLG composites (taken from BDS at 25 °C) and after applied steady shear deformation and recovery (taken from DRD at 200 °C).

FLG, wt. %	Electrical conductivity, S/m					
	PS/PP/FLG	After deformation	After recovery	PP/PS/FLG	After deformation	After recovery
0	5×10^{-14}	1×10^{-10}	1×10^{-10}	5×10^{-14}	1×10^{-10}	1×10^{-10}
1	6×10^{-13}	1×10^{-10}	1×10^{-10}	2×10^{-14}	1×10^{-10}	1×10^{-10}
3	3×10^{-5}	2×10^{-10}	7×10^{-5}	7×10^{-14}	2×10^{-10}	2×10^{-10}
6	3×10^{-4}	8×10^{-10}	5×10^{-4}	7×10^{-8}	6×10^{-10}	2×10^{-5}
9	2×10^{-4}	2×10^{-8}	1×10^{-3}	5×10^{-4}	1×10^{-9}	3×10^{-4}

Table 7. Electrical conductivity data for PP/PS/(FLG/MWCNT) hybrid composites before any deformation (taken from BDS at 25 °C) and after applied steady shear deformation and recovery (taken from DRD at 200 °C).


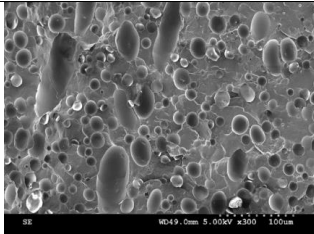
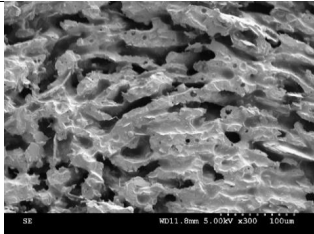
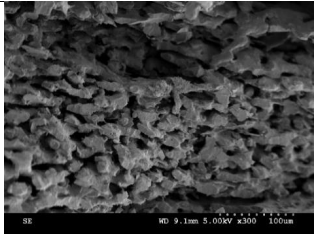
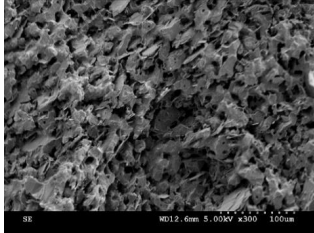
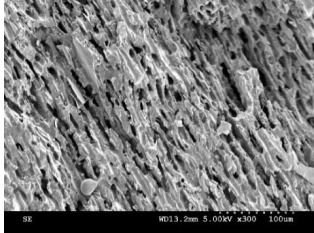
(FLG+MWCNT), wt. %	Electrical conductivity, S/m		
	Before deformation	After deformation	After recovery
1+0.1	3×10^{-6}	4×10^{-10}	6.5×10^{-7}
1+0.3	2×10^{-5}	4×10^{-10}	1.5×10^{-6}
3+0.1	2.9×10^{-6}	6.5×10^{-10}	2×10^{-4}
3+0.3	6×10^{-3}	1.5×10^{-8}	5×10^{-4}

The impact of steady shear deformation on the morphological evolution of both PP/PS/FLG and PS/PP/FLG composites was systematically investigated. Table 8 presents the morphological variations observed in selected composites, including a neat PP/PS 50/50 wt.% blend and PS/PP/FLG composites containing 1 wt.%, 6 wt.%, and 9 wt.% of FLG, after being subjected to 250% shear strain at a shear rate of 1 s^{-1} . The results indicate that the applied deformation had minimal effect on the co-continuous morphology of composites containing FLG concentrations above 3 wt.%. Notably, no significant orientation of the co-continuous structure along the shear direction was observed, contrasting with our previous findings in composites containing only MWCNT, where such orientation was evident [54]. In contrast, for the neat PP/PS blend, the co-continuous morphology transitioned to a drop-in-matrix morphology following the applied deformation. Interestingly, in the PS/PP/FLG composites containing 1 wt.% of FLG, a refinement of the morphology was observed after deformation, an unexpected outcome that warrants further investigation. However, in the case of hybrid PP/PS/(FLG+MWCNT) composites, co-continuous morphology turned to drop-in matrix type morphology after applied steady shear deformation (see results presented in Table 9).

This is the author's peer reviewed, accepted manuscript. However, the online version of record will be different from this version once it has been copyedited and typeset.

PLEASE CITE THIS ARTICLE AS DOI: 10.1063/1.50240789

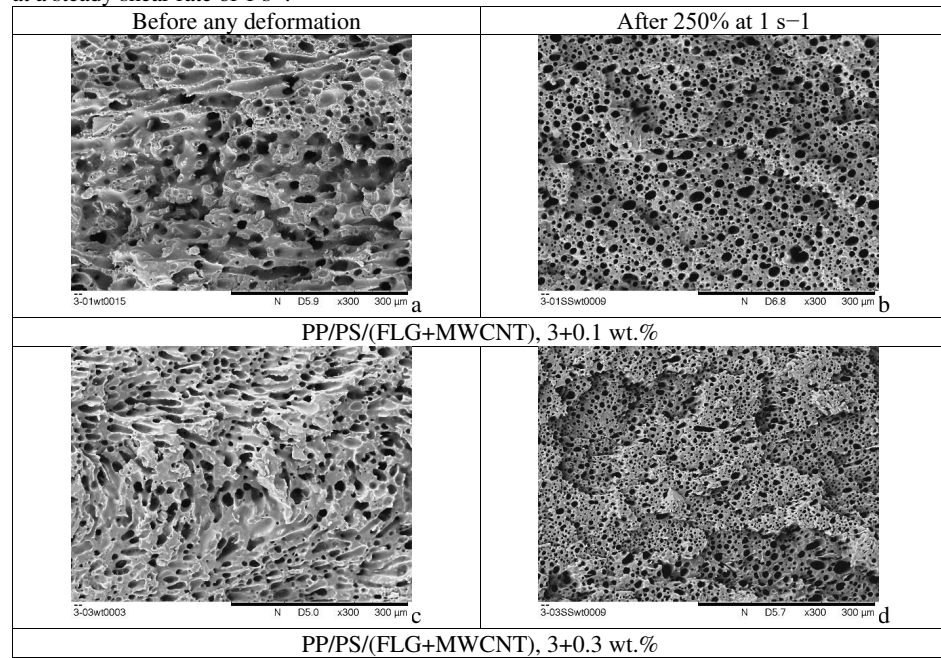
Table 8 – Morphology of a neat PP/PS, 50/50 wt. % blend and chosen PS/PP/FLG composites, containing 1 wt.%, 6 wt.% and 9 wt.% of FLG before any deformation and after 250% of shear strain at a steady shear rate of 1 s^{-1} .

Before any deformation		After 250% at 1 s^{-1}	
PS/PP co-continuous morphology			
			
PS/PP/FLG, 1 wt.% of FLG			
			
PS/PP/FLG, 6 wt.% of FLG			
			
PS/PP/FLG, 9 wt.% of FLG			

This is the author's peer reviewed, accepted manuscript. However, the online version of record will be different from this version once it has been copyedited and typeset.

PLEASE CITE THIS ARTICLE AS DOI: 10.1063/1.50240789

Table 9 – Morphology of chosen PP/PS/(FLG+MWCNT) hybrid composites, containing (3+0.1) wt.% and (3+0.3) wt.% of (FLG+MWCNT) before any deformation and after 250% of shear strain at a steady shear rate of 1 s^{-1} .



Discussion

In our previous research, we demonstrated that the evolution of electrical conductivity and co-continuous blend morphology in composites subjected to steady shear is influenced by several factors, including the concentration of the filler (e.g., carbon nanotubes), the steady shear rate, and the strain amplitude [54]. These variables collectively impact (1) the morphology of the blend, (2) the extent to which conductive nanoparticles cover the interface (interface coverage percentage), as deformation can disrupt the conductive network not only at the polymer interface but throughout the entire material, and (3) the diffusion of conductive nanoparticles toward the interface.

To determine the amount of filler required to establish an electrically conductive network along the co-continuous morphology interface of two polymers, the interface coverage percentage can be calculated. The maximum interface coverage (Σ), assuming that all FLG are at the PP/PS interface can be found as:

$$\Sigma = \frac{A_{FLG}}{S_V \times wt.\%PS} \times 100\% \quad (6)$$

where A_{FLG} is the total area which can cover FLG nanoparticles per mass of FLG in the composite as shown in Figure 9, S_V is the specific interphase area per weight fraction of PS.

To determine the maximum area covered by FLG (A_{FLG}) within the composite, it was assumed that the FLG uniformly covers the entire interface with a dimension of individual particle size composed of 6-10 layers, with each particle in direct contact with its neighbors, without overlapping and agglomeration, as depicted in Figure 9. By knowing the concentration of FLG in the composites, along with their lateral size and density, the number of particles present within the composite was calculated. This, in turn, enabled the estimation of the area occupied by FLG when arranged in the uniform configuration shown in Figure 9.

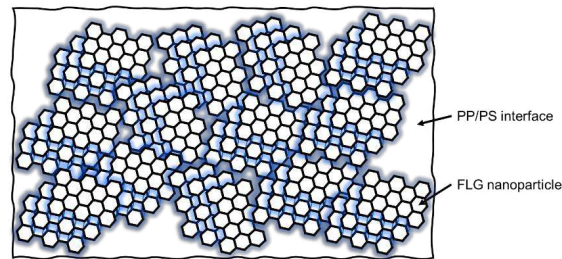


Figure 9 – Schematic of PP/PS interface coverage by connected FLG nanoparticles.

Table 10 presents the FLG weight concentrations, S_V , A_{FLG} , and Σ . The data suggests that full surface coverage of the PP/PS interface can be achieved with FLG concentrations between 3 wt.% and 6 wt.%, resulting in 71% to 143% coverage. Notably, for PS/PP/FLG composites, 71% interface coverage is sufficient to reach the PT concentration. However, for PP/PS/FLG composites, the PT concentration is approximately 6 wt.%, which corresponds to a surface coverage exceeding 100%. This indicates that, at this concentration, the FLG particles may be insufficiently distributed or did not reach the interface to form a continuous electrically conductive network. In comparison, previous research on surface coverage with MWCNT nanoparticles arranged in a triangular array indicated that 0.5 wt.% MWCNT was needed to achieve 113% coverage of the PP/PS interface [54]. At 0.1 and 0.3 wt.% MWCNT, only 23% and 68% coverage were achieved, respectively. However, adding just 0.1 wt.% MWCNT was sufficient to reduce the PT concentration in PP/PS/FLG composites to 1 wt.% FLG. The formation of a continuous FLG-MWCNT-FLG conductive network likely plays a significant role in improving PP/PS interface coverage.

Table 10. Maximum surface coverage of PP/PS co-continuous blend interface by FLG total surface area per wt.% of FLG.

FLG, wt. %	S_V , m ² /g, for neat PP/PS	A_{FLG} , m ²	Σ , %
1		535	24
3	112364	1604	71
6		3209	143
9		4813	214

As demonstrated above, the applied deformation can significantly influence the electrical properties of the investigated composites, what makes it difficult to predict their properties evolution during subsequent processing and post-processing steps. To mitigate these limitations, hybrid composites can be engineered by synergistically combining two different types of carbonaceous nanoparticles. This approach not only enhances the electrical properties and reduces the percolation threshold but also potentially strengthens and stabilizes the conductive filler network, making it more resilient to applied deformations.

Table 11 summarizes several studies from the literature that explore the synergistic effect of CNT mixed with GNP on the electrical conductivity of single polymer matrix composites and polymer blend-based composites. The synergistic effect observed in this study, using FLG and MWCNT in both PP/PS/(FLG+MWCNT) and PS/PP/(FLG+MWCNT) composites, was achieved at lower concentrations of FLG and significantly lower concentrations of MWCNT compared to those reported in the literature. The electrical conductivity values obtained for the concentration range at which the synergistic effect was observed are comparable to those documented in the literature who worked with similar polymer matrices and composite preparation methods.

Table 11. Maximum Synergetic effect (MSE) of CNT+GNP on electrical conductivity.

System	Preparation process	MSE of GNP/CNT, wt. %	σ , S/m, at MSE reached	σ , S/m, at CNT wt. %	σ , S/m, at GNP wt. %	Ref.
PVDF/GNP/CNT	Solution mixing and melt compounding	5/2	30	10^{-5}	-	[40]
SEBS/GNP/CNT	Melt compounding	7/3 5/5	38 84	10 100	10^{-12} 10^{-14}	[41]
EVA/CNT/GNP	Solution mixing	0.7/0.3	10^{-5}	10^{-6}	10^{-9}	[42]
PMMA/MLG/MWCNT	Solvent casting	10/10	10^{-3}	-	10^{-3}	[43]
PVC/MLG/MWCNT		10/10	10^{-8}	-	10^{-9}	
PEI/CNT/GNP	Foams water vapor induced phase separation	1/1	10^{-2}	10^{-3}	-	[48]
ABS/GNP/CNT	Melt compounding	4/2	2	10^{-4}	10^{-13}	[49]
PC/ABS/GNP/MWCNT	Melt-mixing	3/1.5	2	-	10^{-7}	[51]
PP/PS/(FLG+MWCNT)	Conventional melt-mixing	3/0.3	10^{-2}	10^{-8}	10^{-13}	Our work
PS/PP/(FLG+MWCNT)		1/0.3	10^{-4}	10^{-5}	10^{-12}	Our Work

*Ethylene-vinyl acetate (EVA), Poly(methyl methacrylate) (PMMA), multilayered graphene (MLG), Polyvinyl chloride (PVC), Polyethylenimine (PEI), Acrylonitrile Butadiene Styrene (ABS), Polycarbonates (PC).

Conclusions

PP/PS/FLG and PS/PP/FLG blend composites presenting a co-continuous morphology, where FLG was first premixed with PP and PS, respectively, were prepared by melt-mixing using a twin-screw extruder. This was achieved through the dilution of masterbatches of PP/FLG and PS/FLG with PP and PS. Additionally, hybrid composites of PP/PS/(FLG+MWCNT) and PS/PP/(FLG+MWCNT) were prepared following the same processing procedure to investigate the synergistic effects of the FLG and MWCNT mix on electrical properties and percolation threshold

concentration. It was shown that the percolation threshold for the PP/PS/FLG composites was reduced by 65% compared to the PP/FLG composites, and for the PS/PP/FLG composites, it was reduced by 81% compared to the PS/FLG composites. The reduction in the percolation threshold was more significant when FLG was first mixed with the more favorable PS phase: 2 wt.% for the PS/PP/FLG composites compared to 6 wt.% for the PP/PS/FLG composites. It was demonstrated that a synergistic effect on the percolation threshold concentration can be achieved by mixing a small amount of FLG (1 wt.%) with a very low amount of MWCNT (0.1 wt.%), resulting in an 8-order-of-magnitude increase in electrical conductivity, compared to 1 wt.% FLG. The effect of steady shear deformation on the electrical and morphological properties of PP/PS/FLG and PS/PP/FLG blend composites was also investigated. It was shown that the applied deformation can significantly influence the electrical properties of the composites. However, the electrical conductivity for both composites returned to the values observed prior to shear deformation after the recovery step (stress relaxation step). It was also observed that the applied deformation had no significant impact on the co-continuous morphology of the filled composites.

Acknowledgments

Financial support from the Natural Sciences and Engineering Research Council of Canada (NSERC), PRIMA and École de Technologie Supérieure (ÉTS) are gratefully acknowledged. The help of Enzo Godet in rheological measurements by a rotational rheometer is highly appreciated.

Data availability

The data that supports the findings of this study are available within the article.

References

1. Bizhani, H., et al., *Double percolated MWCNTs loaded PC/SAN nanocomposites as an absorbing electromagnetic shield*. European Polymer Journal, 2018. **100**: p. 209-218.
2. Bose, S., et al., *Electrical, rheological and morphological studies in co-continuous blends of polyamide 6 and acrylonitrile-butadiene-styrene with multiwall carbon nanotubes prepared by melt blending*. Composites Science and Technology, 2009. **69**(3-4): p. 365-372.
3. Chen, J., et al., *Design of superior conductive polymer composite with precisely controlling carbon nanotubes at the interface of a co-continuous polymer blend via a balance of π - π interactions and dipole-dipole interactions*. Carbon, 2017. **114**: p. 441-448.
4. Chen, J., et al., *A promising strategy for efficient electromagnetic interference shielding by designing a porous double-percolated structure in MWCNT/polymer-based composites*. Composites Part A: Applied Science and Manufacturing, 2020. **138**: p. 106059.
5. Ellingford, C., et al., *Electrical dual-percolation in MWCNTs/SBS/PVDF based thermoplastic elastomer (TPE) composites and the effect of mechanical stretching*. European Polymer Journal, 2019. **112**: p. 504-514.
6. Liu, T., et al., *Facile preparation of rapidly electro-active shape memory thermoplastic polyurethane/polylactide blends via phase morphology control and incorporation of conductive fillers*. Polymer, 2017. **114**: p. 28-35.
7. Otero-Navas, I., M. Arjmand, and U. Sundararaj, *Carbon nanotube induced double percolation in polymer blends: Morphology, rheology and broadband dielectric properties*. Polymer, 2017. **114**: p. 122-134.

This is the author's peer reviewed, accepted manuscript. However, the online version of record will be different from this version once it has been copyedited and typeset.

PLEASE CITE THIS ARTICLE AS DOI: 10.1063/1.50240789

8. Roman, C., et al., *On the phase affinity of multi-walled carbon nanotubes in PMMA: LDPE immiscible polymer blends*. Polymer, 2017. **118**: p. 1-11.
9. Soares, B.G., et al., *Conducting melt blending of polystyrene and EVA copolymer with carbon nanotube assisted by phosphonium-based ionic liquid*. Journal of Applied Polymer Science, 2018. **135**(24): p. 45564.
10. Soares, B.G., et al., *The effect of the noncovalent functionalization of CNT by ionic liquid on electrical conductivity and electromagnetic interference shielding effectiveness of semi-biodegradable polypropylene/poly (lactic acid) composites*. Polymer Composites, 2020. **41**(1): p. 82-93.
11. Soares da Silva, J.P., et al., *Double Percolation of Melt-Mixed PS/PBAT Blends Loaded With Carbon Nanotube: Effect of Molding Temperature and the Non-covalent Functionalization of the Filler by Ionic Liquid*. Frontiers in Materials, 2019. **6**: p. 191.
12. Yang, Y., et al., *Achieving improved electromagnetic interference shielding performance and balanced mechanical properties in polyketone nanocomposites via a composite MWCNTs carrier*. Composites Part A: Applied Science and Manufacturing, 2020. **136**: p. 105967.
13. Zhang, Q., et al., *Comparison between the efficiencies of two conductive networks formed in carbon black-filled ternary polymer blends by different hierarchical structures*. Polymer Testing, 2017. **63**: p. 141-149.
14. Sun, X.-R., et al., *Effect of phase coarsening under melt annealing on the electrical performance of polymer composites with a double percolation structure*. Physical Chemistry Chemical Physics, 2018. **20**(1): p. 137-147.
15. Soares, B.G., et al., *Effect of double percolation on the electrical properties and electromagnetic interference shielding effectiveness of carbon-black-loaded polystyrene/ethylene vinyl acetate copolymer blends*. Journal of Applied Polymer Science, 2016. **133**(7).
16. Scherzer, S.L., et al., *Phase structure, rheology and electrical conductivity of co-continuous polystyrene/polymethylmethacrylate blends filled with carbon black*. Composites Science and Technology, 2015. **119**: p. 138-147.
17. Qi, X., et al., *Enhanced shape memory property of polylactide/thermoplastic poly (ether) urethane composites via carbon black self-networking induced co-continuous structure*. Composites Science and Technology, 2017. **139**: p. 8-16.
18. Pan, Y., et al., *Enhancing the electrical conductivity of carbon black-filled immiscible polymer blends by tuning the morphology*. European Polymer Journal, 2016. **78**: p. 106-115.
19. Luo, Y., et al., *Preparation of conductive polylactic acid/high density polyethylene/carbon black composites with low percolation threshold by locating the carbon black at the Interface of co-continuous blends*. Journal of Applied Polymer Science, 2021. **138**(17): p. 50291.
20. Gong, T., et al., *Low percolation threshold and balanced electrical and mechanical performances in polypropylene/carbon black composites with a continuous segregated structure*. Composites Part B: Engineering, 2016. **99**: p. 348-357.
21. Gao, C., et al., *High-performance conductive materials based on the selective location of carbon black in poly (ether ether ketone)/polyimide matrix*. Composites Part B: Engineering, 2015. **79**: p. 124-131.

This is the author's peer reviewed, accepted manuscript. However, the online version of record will be different from this version once it has been copyedited and typeset.

PLEASE CITE THIS ARTICLE AS DOI: 10.1063/1.50240789

22. Chen, J., et al., *Balance the electrical properties and mechanical properties of carbon black filled immiscible polymer blends with a double percolation structure*. Composites Science and Technology, 2017. **140**: p. 99-105.
23. Calberg, C., et al., *Electrical and dielectric properties of carbon black filled co-continuous two-phase polymer blends*. Journal of Physics D: Applied Physics, 1999. **32**(13): p. 1517.
24. Bai, L., et al., *Localizing graphene at the interface of cocontinuous polymer blends: Morphology, rheology, and conductivity of cocontinuous conductive polymer composites*. Journal of Rheology, 2017. **61**(4): p. 575-587.
25. Bai, L., et al., *Kinetic control of graphene localization in co-continuous polymer blends via melt compounding*. Langmuir, 2018. **34**(3): p. 1073-1083.
26. Helal, E., et al., *Correlation between morphology, rheological behavior, and electrical behavior of conductive cocontinuous LLDPE/EVA blends containing commercial graphene nanoplatelets*. Journal of Rheology, 2019. **63**(6): p. 961-976.
27. Lan, Y., et al., *Electrically conductive thermoplastic polyurethane/polypropylene nanocomposites with selectively distributed graphene*. Polymer, 2016. **97**: p. 11-19.
28. Mao, C., Y. Zhu, and W. Jiang, *Design of electrical conductive composites: tuning the morphology to improve the electrical properties of graphene filled immiscible polymer blends*. ACS applied materials & interfaces, 2012. **4**(10): p. 5281-5286.
29. Rafeie, O., et al., *Conductive poly (vinylidene fluoride)/polyethylene/graphene blend-nanocomposites: Relationship between rheology, morphology, and electrical conductivity*. Journal of Applied Polymer Science, 2018. **135**(23): p. 46333.
30. Lin, Y., et al., *A highly stretchable and sensitive strain sensor based on graphene-elastomer composites with a novel double-interconnected network*. Journal of Materials Chemistry C, 2016. **4**(26): p. 6345-6352.
31. Mun, S.C., et al., *Strategies for interfacial localization of graphene/polyethylene-based cocontinuous blends for electrical percolation*. AIChE Journal, 2019. **65**(6): p. e16579.
32. Sadeghi, A., R. Moeini, and J.K. Yeganeh, *Highly conductive PP/PET polymer blends with high electromagnetic interference shielding performances in the presence of thermally reduced graphene nanosheets prepared through melt compounding*. Polymer Composites, 2019. **40**(S2): p. E1461-E1469.
33. Shen, Y., et al., *Selective localization of reduced graphene oxides at the interface of PLA/EVA blend and its resultant electrical resistivity*. Polymer Composites, 2017. **38**(9): p. 1982-1991.
34. Huang, J., et al., *Control of carbon nanotubes at the interface of a co-continuous immiscible polymer blend to fabricate conductive composites with ultralow percolation thresholds*. Carbon, 2014. **73**: p. 267-274.
35. Kar, G.P., et al., *Tailoring the dispersion of multiwall carbon nanotubes in co-continuous PVDF/ABS blends to design materials with enhanced electromagnetic interference shielding*. Journal of Materials Chemistry A, 2015. **3**(15): p. 7974-7985.
36. Chen, J., et al., *Trapping carbon nanotubes at the interface of a polymer blend through adding graphene oxide: a facile strategy to reduce electrical resistivity*. Journal of Materials Chemistry C, 2013. **1**(47): p. 7808-7811.
37. Nasti, G., et al., *Double percolation of multiwalled carbon nanotubes in polystyrene/polylactic acid blends*. Polymer, 2016. **99**: p. 193-203.
38. Xu, Z., et al., *Enhancement of electrical conductivity by changing phase morphology for composites consisting of polylactide and poly (ϵ -caprolactone) filled with acid-oxidized*

This is the author's peer reviewed, accepted manuscript. However, the online version of record will be different from this version once it has been copyedited and typeset.

PLEASE CITE THIS ARTICLE AS DOI: 10.1063/5.0240789

- multiwalled carbon nanotubes*. ACS applied materials & interfaces, 2011. **3**(12): p. 4858-4864.
39. Shi, Y., et al., *Simultaneously improved electromagnetic interference shielding and flame retarding properties of poly (butylene succinate)/thermoplastic polyurethane blends by constructing segregated flame retardants and multi-walled carbon nanotubes double network*. Composites Part A: Applied Science and Manufacturing, 2020. **137**: p. 106037.
 40. Xiao, Y.-j., et al., *Hybrid network structure and thermal conductive properties in poly (vinylidene fluoride) composites based on carbon nanotubes and graphene nanoplatelets*. Composites Part A: Applied Science and Manufacturing, 2016. **90**: p. 614-625.
 41. Kuester, S., et al., *Hybrid nanocomposites of thermoplastic elastomer and carbon nanoadditives for electromagnetic shielding*. European Polymer Journal, 2017. **88**: p. 328-339.
 42. Calheiros Souto, L.F. and B.G. Soares, *EVA copolymer loaded with PAni/CNT/GNP hybrids: A flexible and lightweight material with high microwave absorption*. Journal of Applied Polymer Science, 2024. **141**(25): p. e55531.
 43. Joseph, J., et al., *Graphene and CNT filled hybrid thermoplastic composites for enhanced EMI shielding effectiveness*. Materials Research Express, 2019. **6**(8): p. 085617.
 44. Paszkiewicz, S., et al., *Electrically and thermally conductive low density polyethylene-based nanocomposites reinforced by MWCNT or hybrid MWCNT/graphene nanoplatelets with improved thermo-oxidative stability*. Nanomaterials, 2018. **8**(4): p. 264.
 45. Maiti, S. and B. Khatua, *Graphene nanoplate and multiwall carbon nanotube-embedded polycarbonate hybrid composites: High electromagnetic interference shielding with low percolation threshold*. Polymer Composites, 2016. **37**(7): p. 2058-2069.
 46. Palacios, J.K., et al., *Tailoring the rheology and electrical properties of polyamide 66 nanocomposites with hybrid filler approach: graphene and carbon nanotubes*. Polymer international, 2021. **70**(9): p. 1329-1343.
 47. Sun, C., et al., *Constructing high-efficiency microwave shielding networks in multi-walled carbon nanotube/poly (ϵ -caprolactone) composites by adding carbon black and graphene nano-plates*. Polymer International, 2023. **72**(7): p. 619-628.
 48. Abbasi, H., M. Antunes, and J.I. Velasco, *Effects of carbon nanotubes/graphene nanoplatelets hybrid systems on the structure and properties of polyetherimide-based foams*. Polymers, 2018. **10**(4): p. 348.
 49. Dul, S., et al., *Graphene/carbon nanotube hybrid nanocomposites: effect of compression molding and fused filament fabrication on properties*. Polymers, 2020. **12**(1): p. 101.
 50. Bertolini, M.C., et al., *Hybrid composites based on thermoplastic polyurethane with a mixture of carbon nanotubes and carbon black modified with polypyrrole for electromagnetic shielding*. Frontiers in Materials, 2020. **7**: p. 174.
 51. Dos Anjos, E.G., et al., *Role of adding carbon nanotubes in the electric and electromagnetic shielding behaviors of three different types of graphene in hybrid nanocomposites*. Journal of Thermoplastic Composite Materials, 2023. **36**(8): p. 3209-3235.
 52. Chen, J., et al., *Synergistic effect of carbon nanotubes and carbon black on electrical conductivity of PA6/ABS blend*. Composites science and technology, 2013. **81**: p. 1-8.
 53. Strugova, D., et al., *Ultra-Low Percolation Threshold Induced by Thermal Treatments in Co-Continuous Blend-Based PP/PS/MWCNTs Nanocomposites*. Nanomaterials, 2021. **11**(6): p. 1620.

This is the author's peer reviewed, accepted manuscript. However, the online version of record will be different from this version once it has been copyedited and typeset.

PLEASE CITE THIS ARTICLE AS DOI: 10.1063/5.0240789

54. Strugova, D., É. David, and N.R. Demarquette, *Effect of steady shear deformation on electrically conductive PP/PS/MWCNT composites*. Journal of Rheology, 2023. **67**(5): p. 977-993.
55. Vandebril, S., J. Vermant, and P. Moldenaers, *Efficiently suppressing coalescence in polymer blends using nanoparticles: role of interfacial rheology*. Soft Matter, 2010. **6**(14): p. 3353-3362.
56. Thareja, P., K. Moritz, and S.S. Velankar, *Interfacially active particles in droplet/matrix blends of model immiscible homopolymers: Particles can increase or decrease drop size*. Rheologica acta, 2010. **49**(3): p. 285-298.
57. Thareja, P. and S. Velankar, *Rheology of immiscible blends with particle-induced drop clusters*. Rheologica acta, 2008. **47**(2): p. 189-200.
58. Vermant, J., et al., *Coalescence suppression in model immiscible polymer blends by nano-sized colloidal particles*. Rheologica acta, 2004. **43**(5): p. 529-538.
59. Bose, S., et al., *Phase separation as a tool to control dispersion of multiwall carbon nanotubes in polymeric blends*. ACS applied materials & interfaces, 2010. **2**(3): p. 800-807.
60. Genoyer, J., N.R. Demarquette, and J. Soulestin, *Effect of clay particles size and location on coalescence in PMMA/PS blends*. Journal of Rheology, 2019. **63**(6): p. 883-893.
61. Genoyer, J., J. Soulestin, and N.R. Demarquette, *Influence of the molar masses on compatibilization mechanism induced by two block copolymers in PMMA/PS blends*. Journal of Rheology, 2018. **62**(3): p. 681-693.
62. Strugova, D., É. David, and N.R. Demarquette, *Linear viscoelasticity of PP/PS/MWCNT composites with co-continuous morphology*. Journal of Rheology, 2022. **66**(4): p. 671-681.
63. Palierne, J., *Linear rheology of viscoelastic emulsions with interfacial tension*. Rheologica acta, 1990. **29**(3): p. 204-214.
64. Gramespacher, H. and J. Meissner, *Interfacial tension between polymer melts measured by shear oscillations of their blends*. Journal of Rheology, 1992. **36**(6): p. 1127-1141.
65. Bousmina, M., *Effect of interfacial tension on linear viscoelastic behavior of immiscible polymer blends*. Rheologica acta, 1999. **38**(3): p. 251-254.
66. Souza, A.M.C.d., P.S. Calvao, and N.R. Demarquette, *Linear viscoelastic behavior of compatibilized PMMA/PP blends*. Journal of applied polymer science, 2013. **129**(3): p. 1280-1289.
67. Omonov, T., et al., *Phase continuity detection and phase inversion phenomena in immiscible polypropylene/polystyrene blends with different viscosity ratios*. Polymer, 2007. **48**(20): p. 5917-5927.
68. Yu, W., W. Zhou, and C. Zhou, *Linear viscoelasticity of polymer blends with co-continuous morphology*. Polymer, 2010. **51**(9): p. 2091-2098.
69. Kou, Y., et al., *Robust networks of interfacial localized graphene in cocontinuous polymer blends*. Journal of Rheology, 2021. **65**(6): p. 1139-1153.
70. Bird, R.B., R.C. Armstrong, and O. Hassager, *Dynamics of polymeric liquids. Vol. 1: Fluid mechanics*. 1987.
71. Carreau, P.J., D.C. De Kee, and R.P. Chhabra, *Rheology of polymeric systems: principles and applications*. 2021: Carl Hanser Verlag GmbH Co KG.
72. Bousmina, M., A. Ait-Kadi, and J. Faisant, *Determination of shear rate and viscosity from batch mixer data*. Journal of rheology, 1999. **43**(2): p. 415-433.

This is the author's peer reviewed, accepted manuscript. However, the online version of record will be different from this version once it has been copyedited and typeset.

PLEASE CITE THIS ARTICLE AS DOI: 10.1063/1.50240789

73. Kohlgrüber, K., *Co-Rotating Twin-Screw Extruders - Fundamentals, Technology, and Applications*. Vol. Chapter 3: Rheological Properties of Polymer Melts. 2008: Carl Hanser Verlag GmbH & Co. KG. 367.
74. Jordhamo, G., J. Manson, and L. Sperling, *Phase continuity and inversion in polymer blends and simultaneous interpenetrating networks*. *Polymer Engineering & Science*, 1986. **26**(8): p. 517-524.
75. Chen, J., et al., *Combined effect of compatibilizer and carbon nanotubes on the morphology and electrical conductivity of PP/PS blend*. *Polymers for advanced technologies*, 2014. **25**(6): p. 624-630.
76. Hwang, T.Y., Y. Yoo, and J.W. Lee, *Electrical conductivity, phase behavior, and rheology of polypropylene/polystyrene blends with multi-walled carbon nanotube*. *Rheologica acta*, 2012. **51**(7): p. 623-636.
77. Mucha, M., J. Marszałek, and A. Fidrych, *Crystallization of isotactic polypropylene containing carbon black as a filler*. *Polymer*, 2000. **41**(11): p. 4137-4142.
78. Assouline, E., et al., *Nucleation ability of multiwall carbon nanotubes in polypropylene composites*. *Journal of Polymer Science Part B: Polymer Physics*, 2003. **41**(5): p. 520-527.
79. Kalaitzidou, K., et al., *The nucleating effect of exfoliated graphite nanoplatelets and their influence on the crystal structure and electrical conductivity of polypropylene nanocomposites*. *Journal of materials science*, 2008. **43**: p. 2895-2907.
80. Filippone, G. and M. Salzano de Luna, *A unifying approach for the linear viscoelasticity of polymer nanocomposites*. *Macromolecules*, 2012. **45**(21): p. 8853-8860.
81. Filippone, G., et al., *Assembly of plate-like nanoparticles in immiscible polymer blends—effect of the presence of a preferred liquid–liquid interface*. *Soft Matter*, 2014. **10**(18): p. 3183-3191.
82. Altobelli, R., M.S. de Luna, and G. Filippone, *Interfacial crowding of nanoplatelets in co-continuous polymer blends: Assembly, elasticity and structure of the interfacial nanoparticle network*. *Soft Matter*, 2017. **13**(37): p. 6465-6473.
83. Galloway, J.A., M.D. Montminy, and C.W. Macosko, *Image analysis for interfacial area and cocontinuity detection in polymer blends*. *Polymer*, 2002. **43**(17): p. 4715-4722.
84. Veenstra, H., et al., *On the mechanical properties of co-continuous polymer blends: experimental and modelling*. *Polymer*, 2000. **41**(5): p. 1817-1826.